Int J Adv Manuf Technol (2017) 92:3883–3901
DOI 10.1007/s00170-017-0444-5

ORIGINAL ARTICLE

A new machining strategy for roughing deep pockets of magnesium-rare earth alloys

Frederic Monies[1] · Isabelle Danis[1] · Christian Bes[1] · Sonia Cafieri[2] · Marcel Mongeau[2]

Received: 20 January 2017 / Accepted: 20 April 2017 / Published online: 5 May 2017

Abstract Plunge milling is an efficient machining process for roughing deep pockets. Its efficiency is mainly due to low radial forces on the cutter. This leads to reduced bendings and vibrations that allow one to improve cutting parameter values. The machining time can then be reduced with respect to machining processes with constant Z-level. Recently, another machining process has been introduced, called "balancing of the transversal cutting force" (BotTCF), that is also characterized by a suitable distribution of forces on the cutter. It has been applied only to finishing operations on complex surfaces. In this paper, we present two main contributions. First, we extend the BotTCF concept to roughing open deep pockets and semi-open pockets opened from side to side. This is mainly based on successive parallel ramping trajectories, defined by an optimal angle which ensures a good balancing of the transversal cutting forces. This can be applied to 3-axis and 5-axis computer numerical control (CNC) machine tools. Second, we propose a new, hybrid methodology for roughing semi-open pockets (not opened from side to side) and closed pockets. It is based on the combination of ramping trajectories with BotTCF and plunge milling. The proposed methodology is developed for three-axis machining and can be extended to five-axis machining. Based on an identical criterion (identical maximum force acting on the cutters), we perform a fair machining-time comparison of plunge milling with the proposed hybrid method applied on a closed deep pocket: a simplified aeronautical housing made of magnesium-rare earth alloy. Results show a significant gain in machining time when the hybrid method is applied.

Keywords Roughing · Pocket milling · Plunge milling · Ramping · Mg-Zr-Zn-RE alloy

1 Introduction

In industry, notably in aeronautics, roughing deep pockets efficiently is a crucial issue. In the case of *low-stiffness* cutters (low diameter-length ratio), a suitable distribution of forces acting on them is necessary to ensure an effective process. Otherwise, the set of possible values of the cutting parameters (cutting speed, feed per tooth, depth of cut, etc.) must be restricted so as to prevent bendings and vibrations.

Plunge milling [1, 2] is a recognized efficient machining process for roughing deep pockets. It involves a series of successive plunge cycles (Fig. 1) into the material. One cycle is composed of three phases: a *plunging phase*, where the tool removes material while going down; a *rising phase*, performed in rapid motion, where the tool goes up; and finally, an *offset phase* (above the stock), also carried out in rapid motion, to position the cutter before beginning a new cycle. The distance between two successive plunges into the stock is called the *radial offset*, ae, and is therefore directly related to the number of plunges. Plunge milling efficiency is mainly due to low radial forces on the cutter, whatever workpiece material is considered. This leads to reduced bendings and vibrations [3, 4] that allows one to improve cutting parameter values. Plunge milling is especially interesting in the case of a cutter featuring low stiffness. It is recognized to be particularly efficient for machining hard

✉ Frederic Monies
frederic.monies@univ-tlse3.fr

[1] Université de Toulouse 3; ICA (Institut Clément Ader), 31062 Toulouse, France

[2] ENAC, MAIAA, 31055 Toulouse, France

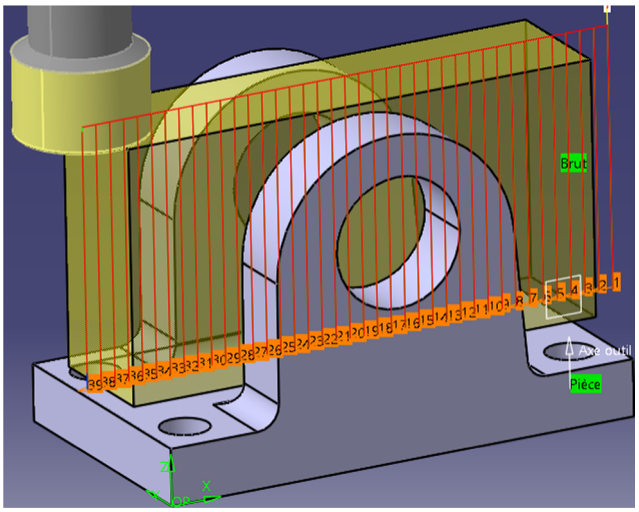

Fig. 1 Plunge milling operation with 39 successive plunge cycles, on a semi-open pocket opened from side to side

materials because of the high axial forces acting on the cutter [4, 5]. Nevertheless, even in the case of light materials like magnesium alloys, its efficiency has been proved, although axial forces are not the preponderant ones [6–8].

Another machining process, recently introduced by [9, 10] for finishing complex surfaces, is the so-called *Balancing of the transversal cutting force* (BotTCF). Its efficiency relies on the well-balanced distribution of the cutting forces on the cutter. BotTCF is applicable for all type of materials and can be used with toroidal cutters with round inserts, as in [9–13] or with pocket milling cutters, as in [14]. BotTCF imposes to incline the cutter axis towards the back of the cutter with respect to the feed direction (negative tool axis inclination) [14]. It can be realized on 5-axis computer numeric control (CNC) machine tools by tilting the cutter axis; or by inclining the workpiece, or the tool path trajectories on 3-axis CNC machine tools (see Fig. 2).

To obtain maximum efficiency, the cutter has to be engaged in full slotting. In this case, all inserts constantly work simultaneously. Then, an optimal inclination of the cutter axis (*balanced angle*) can be computed to balance the transversal cutting force that acts on the cutter, as in [14]. The transversal component of the cutting force is defined as the cutting force component perpendicular to the programmed feedrate vector V_f. This inclination allows one to reduce deflection and also vibrations with a better dynamic cutter behavior.

Monies et al. [14] show that the amplitude of the transversal component can be reduced by a factor larger than five, when compared with milling with no cutter-axis inclination. They also find that the amplitude of the force component in the feed direction is greatly reduced with the balanced angle. This study considers pocket milling cutters in the case of a magnesium alloy MRI301F (Mg-Nd-Y-Zr-Zn). Therefore, for the same maximal tool loading, better cutting conditions can be taken with BotTCF (for example, by increasing the feed per tooth and/or the total axial depth of cut). This can reduce the total machining time (by increasing the tool displacement feed and/or reducing the number of tool paths), compared with machining without tool-axis inclination. Hence, BotTCF can increase productivity.

The first contribution of this paper is to extend the BotTCF concept, up to now only used for finition purposes,

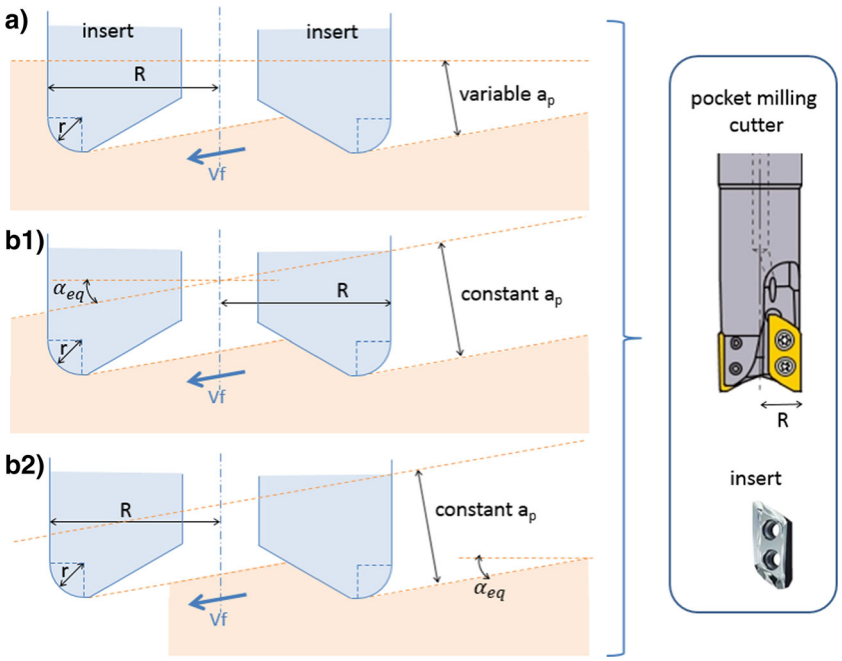

Fig. 2 Ramping motion of a pocket milling cutter into the material with cutter radius R and round corner radius r. **a** First pass with a variable a_p, **b1** Following passes with a constant a_p, **b2** End of ramping: the cutter needs to be cleared out of the material

to roughing deep pockets in an industrial context. To this purpose, we choose to concentrate on pocket milling cutters, because they are commonly used for this type of workpieces. Successive parallel ramping passes involving an optimal (balanced) inclination angle, implemented as in [14], are then used. This permits to balance the transversal cutting force. We call this original strategy: *BotTCF Ramping*. This extension is then adapted to, and its efficiency is demonstrated on three types of pockets: open pockets, semi-open pockets, and closed pockets without islands. However, for semi-open pockets not opened from side to side and closed pockets, BotTCF Ramping cannot be directly applied. Indeed, we show that the pocket milling cutter must end its paths in a material-free space whose width is at least the tool diameter. This motivates our second contribution: the use of plunge milling for initial material removal along the pocket walls (the remaining pocket material being then removed with BotTCF Ramping). We call this overall coupling strategy *Hybrid BotTCF Ramping* (HBR). The benefits of HBR compared to traditional plunge milling are shown on a closed pocket.

In this study, the machined material is a magnesium-rare earth alloy, MRI301F (Mg-Nd-Y-Zr-Zn), chosen for its advantageous properties (low density and good mechanical features). It can be used at temperatures up to 200 °C and is well fitted to aeronautical applications. The composition of this alloy, its properties, and its machinability are presented in the studies conducted by Danis et al. [6–8, 14].

The paper is organized as follows. Section 2 introduces BotTCF Ramping and defines the ramping trajectories following the BotTCF balanced-angle criterion for roughing open deep pockets and semi-open pockets opened from side to side. In Section 3, we introduce the HBR milling strategy in order to deal with semi-open pockets not opened from side to side, and closed pockets, both of which cannot be addressed directly by BotTCF Ramping. In Section 4, we present the cutting-force models that permit to evaluate the forces acting on the plunge milling cutter and on the pocket milling cutter. These models are used later to determine the cutting conditions. Based on an identical criterion (identical maximum force acting on the cutters), Section 5 presents a fair machining-time comparison of crude plunge milling with the introduced HBR methodology on a closed deep pocket: a simplified aeronautical housing made of magnesium-rare earth alloy. Finally, we present conclusions and perspectives in Section 6.

2 BotTCF ramping

This section introduces BotTCF Ramping and explains it for the cases of open deep pockets and semi-open pockets opened from side to side.

2.1 General concept

Traditionally, *ramping* refers to the initial, short trajectory of the cutter entering the material, with an increasing depth of cut. It is usually followed by a constant Z-level milling strategy.

BotTCF refers to a physical model and to a criterion to choose a balanced angle, introduced in [14], so as to minimize the transversal cutting force. BotTCF can be realized on 5-axis computer numeric control (CNC) machine tools by tilting the cutter axis. It can also be realized on 3-axis CNC machine tools by inclining the workpiece or the tool path trajectories.

In this paper, we propose a new roughing strategy that we call *BotTCF Ramping*, and we present its application to the machining of open deep pockets. Contrary to traditional ramping, BotTCF Ramping is a roughing process that relies on the definition of entire tilted milling trajectories. These trajectories are parallel, separated by a depth-of-cut value a_p, and tilted by an angle $(90°+\alpha_{eq})$ relative to the cutter axis. This angle is chosen so as to minimize the transversal cutting force, in accordance with the BotTCF criterion.

Figure 2 illustrates the phases of BotTCF Ramping (here with a pocket milling cutter on a 3-axis CNC machine tool). First, Fig. 2a shows the first pass featuring an initial descent of the cutter into the material following a ramp with an *increasing* depth of cut a_p. Figure 2b1 and b2 display the following (parallel) passes. The cutter still follows descending trajectories into the material but the depth of cut a_p remains constant.

Remark that BotTCF Ramping can only be applied to open pockets or semi-open pockets geometries with multiple open edges. Indeed, Fig. 2b2 shows that at the end of each trajectory, the cutter needs to be cleared out of the material while removing the remaining uncut material under the cutter, without damaging the worpiece.

In the next subsection, we present the application of BotTCF Ramping to open deep pockets and semi-open pockets opened from side to side.

2.2 Open deep pockets and semi-open pockets opened from side to side

For the sake of simplicity, we first explain the overall BotTCF Ramping methodology for the case of an elementary semi-open pocket opened from side to side. Figure 3 illustrates such an elementary deep pocket. The stock we consider here is a rectangular parallelepiped whose width (its smaller dimension) is slightly larger than the cutter diameter. The parallelepipedic stock represented in yellow color is located between the two vertical walls. To fullfill the BotTCF criterion (i.e., balancing the transversal cutting force acting on the cutter), the cutter trajectories are defined

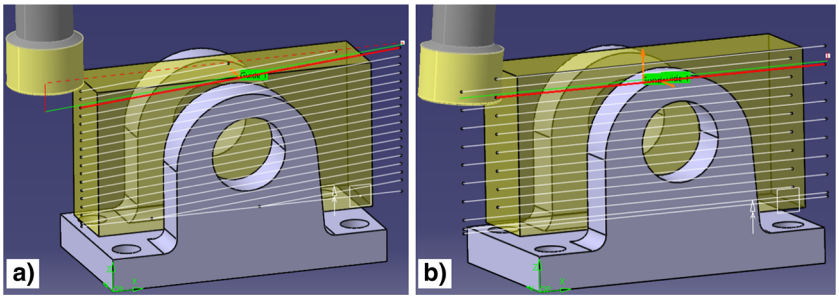

Fig. 3 **a** Ramping with BotTCF by inclining the tool path trajectories (3-axis). **b** Ramping with BotTCF by tilting the cutter axis (5-axis)

on a plane centered with respect to the width of the material to be removed.

This methodology will be extended to more complex deep pockets in the next section. Section 3 not only extends the methodology to the case of wider stocks, it also discusses how to choose the cutter path connecting a sequence of trajectories located on multiple parallel planes. This cutter path will be chosen so as to reduce the cutter movements outside the material (carried out in rapid motion), and thereby the machining time.

The trajectories of the BotTCF Ramping are defined by the following phases:

1. First, we define the planes where the trajectories have to be generated. In the case of the illustrative exemple of Fig. 3, only one plane is necessary.
2. Second, we define, for each plane, four *boundary lines* (dashed lines in red color on Fig. 4) defining a *boundary rectangle* as follows:
   - a top horizontal line, located at a height noted h_s above the stock,
   - a bottom horizontal line, delimitating the bottom of the stock (floor)
   - a starting-point vertical line, located $2R + \delta$ outside the stock (where R is the cutter radius, and δ is a small value that ensures a safe separation of the cutter away from the stock)
   - an ending-point vertical line, located oppositly, δ outside the stock.
3. Third, we define parallel *guide lines* separated from each other by a common constant distance a_p (depth of cut). These guide lines are tilted on 3-axis CNC machine tools (Fig. 3a), but should be horizontal on 5-axis CNC machine tools (Fig. 3b) by tilting the cutter. For both machine types, the involved tilting angle, α_{eq}, is to be computed following the BotTCF criterion. These guide lines set the location of the cutter-contact (CC) points (Figs. 4 and 5). The mathematical formulations of the BotTCF criterion will be provided in Section 4.0.2.
4. We then define the first guide line as follows. Without loss of generalty, we assume that the cutter moves

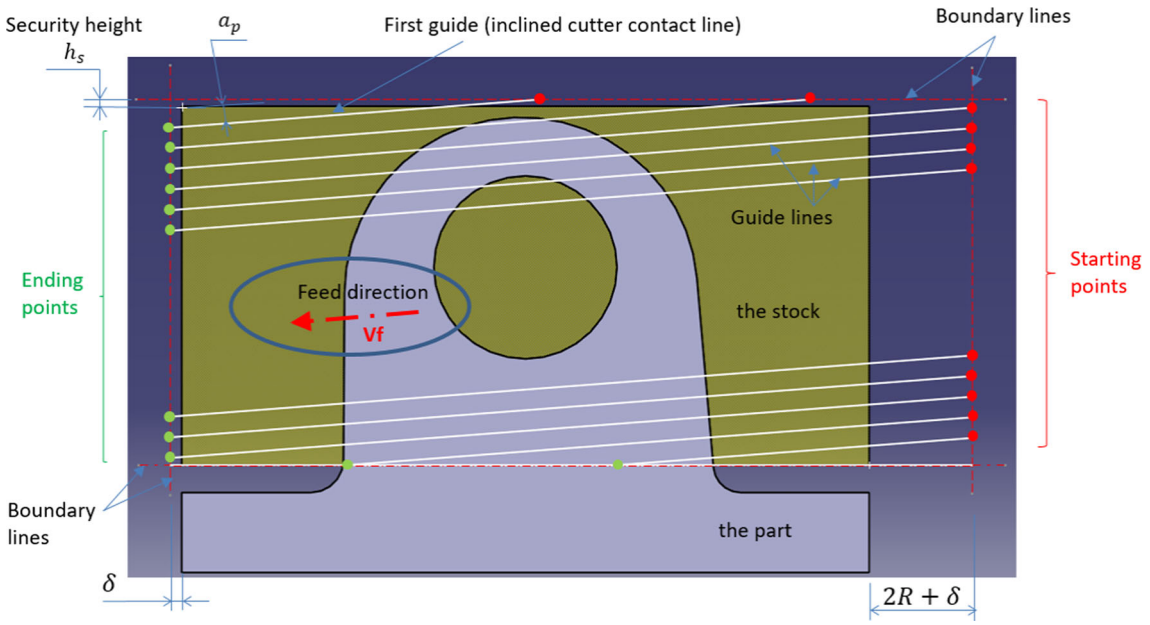

Fig. 4 Guide line trajectories in the case of three-axis machining

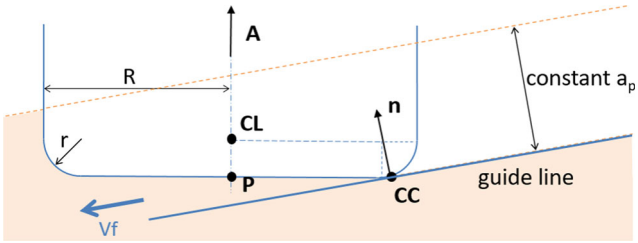

Fig. 5 Key points of the cutter trajectories

(along the guide lines) from the right-hand side to the left-hand side (as on Figs. 3, 4 and 6). The first guide line is at a distance a_p below the top left-hand side corner of the stock. The other parallel guide lines (below) are successively defined at distance a_p from each other.

5. The starting and ending points are located at the intersections of the guide lines with the boundary rectangle, as illustrated in Fig. 4.
6. During the milling, the cutter position is tangent to the guide line (Fig. 5). More precisely, let **CC** denotes the position of the cutter contact point, **CL** denotes the corresponding cutter location point. We have:

$$\mathbf{CL} = \mathbf{CC} + r \cdot \mathbf{n} + (R - r) \cdot \frac{\mathbf{A} \wedge (\mathbf{n} \wedge \mathbf{A})}{||\mathbf{A} \wedge (\mathbf{n} \wedge \mathbf{A}||} \quad (1)$$

where **n** is the normal to the guide at point **CC**, **A** is the cutter axis, R is the cutter radius, and r is the round-corner radius. Note that for 3-axis machining, **A** corresponds to the machine spindle axis.

The position of the point controled by the CNC machine, noted **P**, is given by:

$$\mathbf{P} = \mathbf{CL} - r \cdot \mathbf{A} \quad (2)$$

These **P** points usually define the cutter trajectories driven by the CNC machine tool.

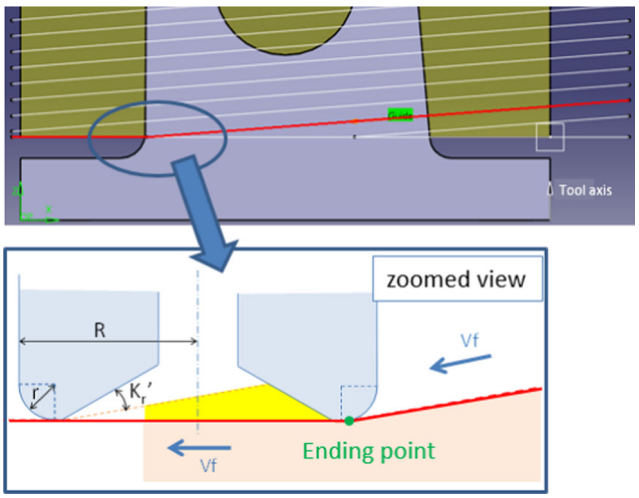

Fig. 6 A ramping (*downward*) trajectory followed by an horizontal trajectory for cutting the remaining material at the (*green-color*) ending point

Remarks:

- BotTCF Ramping can be efficiently applied only in the case where the cutter is completely inside the material (full slotting) or centered. Otherwise, the transversal cutting forces cannot be balanced. These forces are unbalanced when the cutter enters the material and when it finishes its trajectory. As a consequence, in order to take advantage of BotTCF Ramping, the length of the trajectories has to be at least twice larger than the cutter diameter.
- Beyond the ending points located on the bottom horizontal line (Figs. 4 and 6), the cutter must follow an horizontal trajectory. This horizontal trajectory permits to remove the remaining material (illustrated in yellow color on Fig. 6) located under the cutter.
- In 5-axis machining, the guide lines are horizontal. Then, the cutter axis is tilted towards the back of the cutter (with respect to the feed direction, defined by V_f). The tilted angle is defined according to the BotTCF criterion. Using machines with a rotary head, the feed directions are then reversed at each successive parallel ramping passes, reducing thereby cutter movements outside the material (carried out in rapid motion). Otherwise, for 5-axis machines with dual rotary tables, 3-axis machining is more efficient (indeed, in this case, rotary table C rotates 180°, and the cutter has to move, outside the material, at the opposite from its current position in order to start a new trajectory).

  Whatever 5-axis cinematic machine is considered, the last trajectory generally features a depth of cut smaller than the previous (constant) depth of cut a_p. Thus, a new balanced angle has to be defined using the BotTCF criterion for milling the remaining material.

3 HBR: hybrid BotTCF ramping

This section introduces the HBR milling strategy in order to deal with semi-open pockets not opened from side to side, and closed pockets, both of which cannot be addressed directly by BotTCF Ramping. Figure 7 illustrates

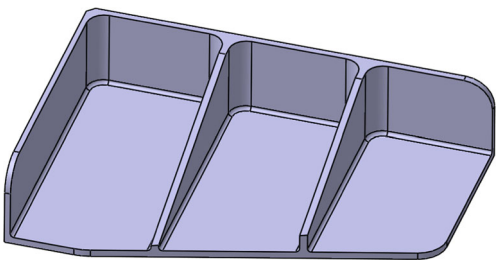

Fig. 7 Example of a workpiece with three semi-open pockets

an aeronautical workpiece composed of semi-open pockets that are not opened from side to side. For this workpiece, the cutter can be fully disengaged from the material at the bottom of the ramp trajectory (Figs. 2c and 8b). This is a necessary condition to apply BotTCF Ramping: the pocket milling cutter must end its trajectory in a material-free space whose width is at least the tool diameter. Moreover, applying directly BotTCF Ramping on such semi-open pockets would require milling the material vertically, so as to reach the starting points that are within the material in the vicinity of the pocket wall. However, the pocket milling cutter is not designed to enter the material vertically on a significative depth of cut. Therefore, BotTCF Ramping cannot be straightforwardly applied on semi-open pockets. For closed pockets (an exemple of such a workpiece is given on Fig. 12), this drawback is even more critical, as both the beginning and the end of the cutter trajectory are not material free.

One of the main contributions of this paper is the idea of introducing an initial milling process that removes the material along the pocket walls, enabling thereby one to use the BotTCF Ramping strategy on the remaining material. In other words, this initial milling process reduces the problem of roughing semi-open or closed pockets to the case of open pockets (discussed in Section 2.2) on which BotTCF Ramping can then be applied. We call this overall coupling strategy: *Hybrid BotTCF Ramping* (HBR). The remaining of this section is dedicated to the description of the HBR strategy applied to semi-open and closed pockets.

3.1 Semi-open deep pockets (not opened from side to side)

Among the various possibilities for the initial milling process to remove the material along the pocket walls, we select plunge milling, as plunge milling is an efficient machining process for roughing deep pockets, thanks to low radial forces on the cutter. This leads to reduced bendings and vibrations that enables one to choose efficient values of the cutting parameters which, in turn, yields reduced machining time. The first phase of HBR is therefore constituted by some plunge milling steps to remove the material along the pocket walls. The initial plunge milling must be performed with a cutter whose diameter is strictly larger than that of the pocket milling cutter used for BotTCF Ramping. Once these plunge milling steps have been performed, the pocket milling cutter can access vertically the starting points in rapid motion, on a material-free space (safely away from the stock and the workpiece). As an example, a plunge milling operation with a 33mm-diameter cutter can be followed by a BotTCF Ramping operation with a 32mm-diameter pocket milling cutter.

Remarks:

- For hard materials, the cutter should be moved away from the vertical wall before the rising phase to avoid any friction with the material. If the rising phase of plunge milling is performed in rapid motion, the cutter inserts will be damaged due to the friction with the material [15, 16]. Then, the rising phase has to be performed in slow motion, which is a serious drawback for the efficiency of this first phase in terms of machining time. Beside, for magnesium-rare earth alloys it has been proved that the rising phase can be carried out in rapid motion (without first moving away the cutter from the vertical wall) without damaging the cutter inserts [6, 7]. This feature is essential to apply plunge milling along the pocket walls.
- Note that if the cutter is not a center-cut end mill, an initial drill operation is necessary to start plunge milling, with for example an indexable drilling tool.

The second phase of HBR consists in BotTCF Ramping. We describe in the following how this process is carried out using trajectories on multiple parallel planes. For illustrating

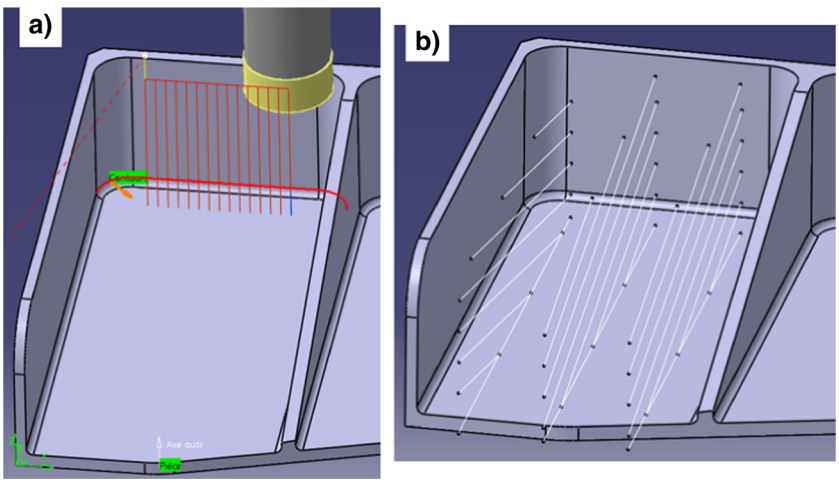

Fig. 8 **a** Plunge milling. **b** BotTCF Ramping: 3 planes

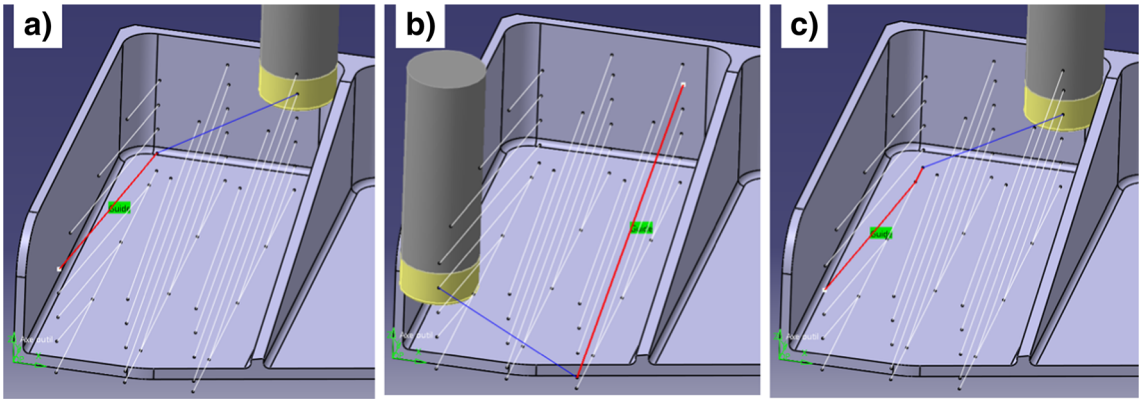

Fig. 9 Representation of successive cutter trajectories during the rectangular cycle, from **a** to **c** with both programmed feedrate motion (*red*) and rapid motion (*blue*)

the method, we consider a pocket milling cutter diameter that allows one to define at least three BotTCF Ramping planes (parallel to each other and parallel to the side walls of the stock), where the trajectories are generated (Figs. 8b and 11). At least, one plane or strictly more than two planes are necessary for BotTCF Ramping to be efficient. This efficiency indeed relies on the well-balanced distribution of the cutting forces on the pocket milling cutter. The cutter has therefore to be centered with respect to the material to be removed, or has to be in full slotting. This cutter configuration is impossible with two planes (Fig. 9).

We describe now the three-plane case which can be straigthforwardly generalized to more planes. One plane is located at the center of the stock and the two others (*side planes*) are equidistant from the central plane, and located on either side of it (Fig. 10).

For semi-open pockets, we can consider two types of workpiece: parallel side walls (see Fig. 11) and no parallel side walls (see Fig. 13). In the first case (see Fig. 11), the initial plunge milling is used only to remove the material along the back wall (see Fig. 8a). In the second case (see Fig. 13), the initial plunge milling is used to remove the material along all the pocket walls that are not rectilinear. For the latter, the milling methodology is the same as for closed pockets and will be described in Section 3.2.

In this subsection, we discuss only the first type of workpieces (parallel side walls). Concerning the two parallel side planes presented above (numbered 2 and 3 on Fig. 11), they have to be located at a distance equal to the cutter radius from the side walls of the stock. The central plane (numbered 1) is located at the middle of the two parallel side planes.

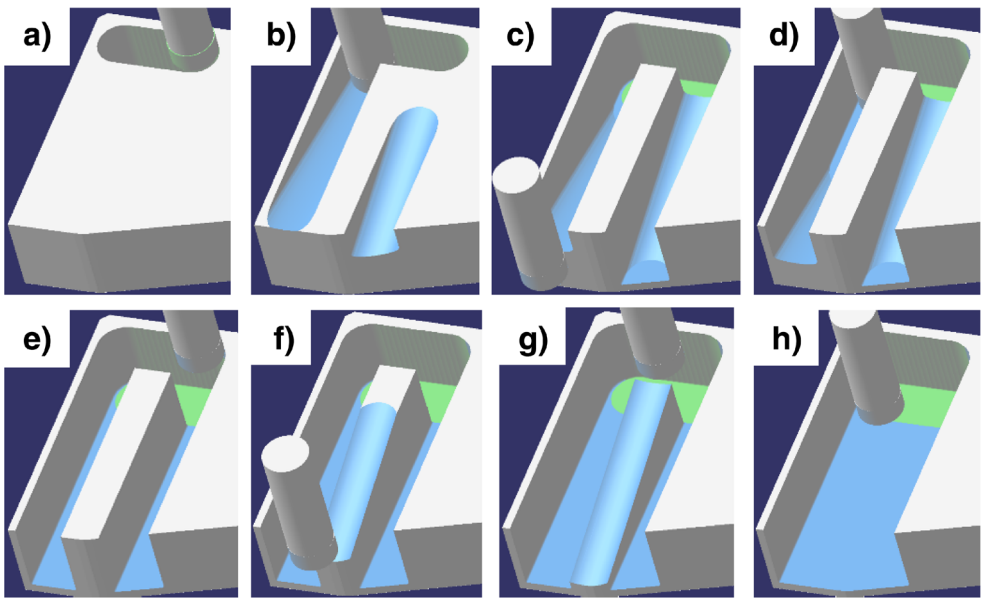

Fig. 10 Simulation of material removal during the successive tool displacements

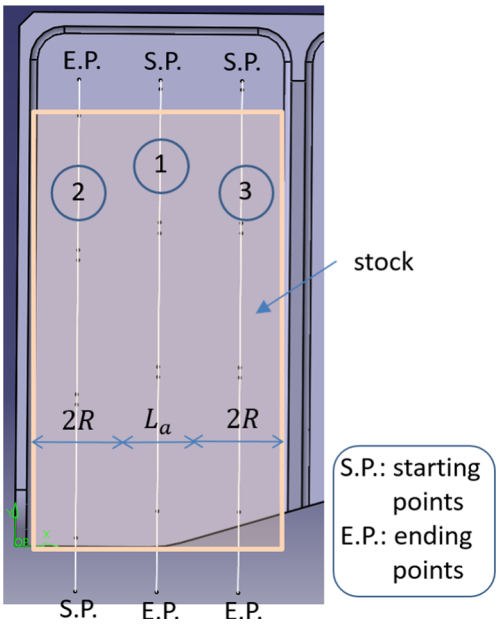

Fig. 11 Construction of three planes containing the machining trajectories

In each plane, the trajectories of BotTCF Ramping are defined (Fig. 8b, for our example) according to the phases presented in Section 2.2.

The milling is then carried out in full slotting for the trajectories associated with planes 2 and 3. The cutter is centered with respect to the material to be removed for the trajectories associated with plane 1 (width L_a on Fig. 11, with $L_a < 2R$). As mentioned above, this ensures the efficiency of BotTCF Ramping.

In order to optimize the machining time, we propose first to mill successively along the trajectories of planes 2 and 3, in opposite directions. This means that the starting points of plane 2 and the ending points of plane 3 are on a same side, and thus the starting points of plane 3 and the ending points of plane 2 are on the opposite side (see Fig. 11). This permits a rectangular cycle of ramping trajectories (Fig. 9), thus reducing the cutter movements outside the material (carried out in rapid motion), and thereby the machining time. When the milling of all ramping trajectories in planes 2 and 3 is completed, one performs the milling along the ramping trajectories of plane 1.

An overall simulation of the material removal using the new HBR methodology is presented in Fig. 10 for a workpiece with parallel side walls. When the stock width is sufficiently large, more than three BotTCF Ramping planes can be defined. For example, in the case of four planes (Figs. 15 and 16), two successive rectangular cycles of ramping trajectories are used in order to reduce the cutter movements outside the material. The first rectangular cycle involves planes 1 and 3, and the second rectangular cycle involves planes 2 and 4. The efficiency of the HBR strategy with two successive rectangular cycles will be discussed in more detail for closed pockets in Section 3.2.

Next, we describe the HBR methodology for closed pockets. This methodology is more general and can also be applied to any geometry of open and semi-open pockets, including cases with non parallel side walls, that were not treated in this subsection.

3.2 Closed deep pockets

For describing the HBR methodology, we consider a workpiece corresponding to a simplified aeronautical housing. This workpiece consists of two pockets (see Fig. 12). We start by applying HBR to pocket 1.

In the first phase of the HBR methodology, plunge milling begins to remove material along the pocket walls (Fig. 13a, b). Then, plunge milling is again applied to obtain a remaining stock with two parallel side walls (Fig. 13c, d). These two plunge milling phases are carried out with a cutter whose diameter is strictly larger than that of the pocket milling cutter. In the second phase of HBR, BotTCF Ramping is applied.

For illustrating the method, we consider a pocket milling cutter diameter that allows one to define, from the remaining stock, at least three BotTCF Ramping planes (Fig. 13e and f) where the trajectories are generated. The milling is then performed in full slotting for the trajectories associated with plane 1. The cutter is centered with respect to the material to be removed for the trajectories associated with planes 2 and 3 (width L_a, with $L_a < 2R$). This ensures a good balance of the transversal cutting force. In order to optimize the machining time, we propose to mill first in full slotting along the trajectories of plane 1 (Fig. 14a, b). Once the material along plane 1 is removed, the milling is applied successively along the trajectories of planes 2 and

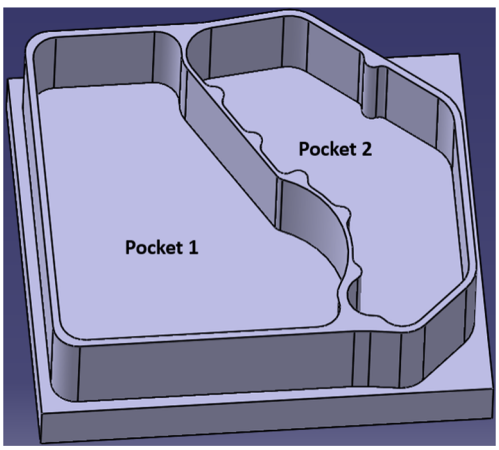

Fig. 12 Aeronautical housing consisting of two closed pockets

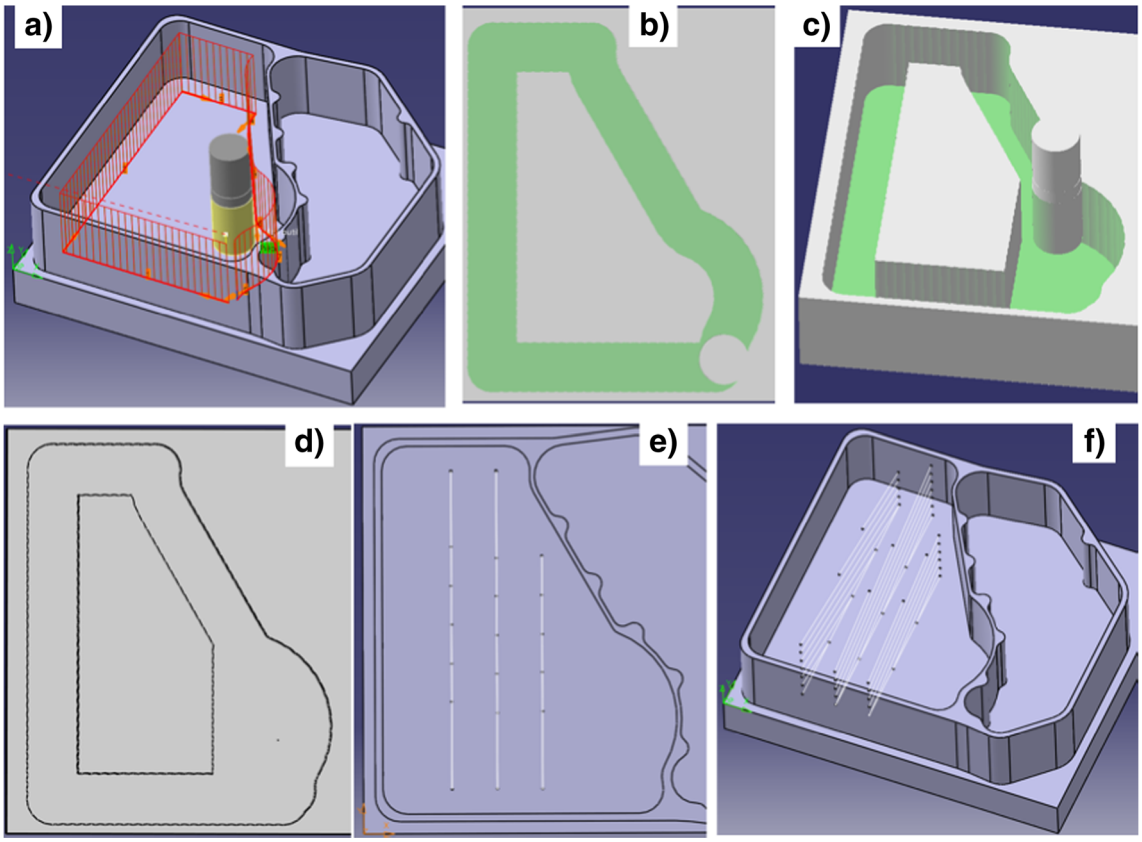

Fig. 13 Plunge milling and BotTCF ramping (orders of operations: from **a** to **f**)

3 (Fig. 14c, d). This permits to make a rectangular cycle of ramping trajectories and reduces the cutter movements outside the material (carried out in rapid motion), and thereby the machining time.

An overall simulation representing the different steps of HBR material removing is illustrated on Fig. 14.

In the case of pocket 1 in our example, the left-hand side wall is rectilinear. Then, it is possible to define another

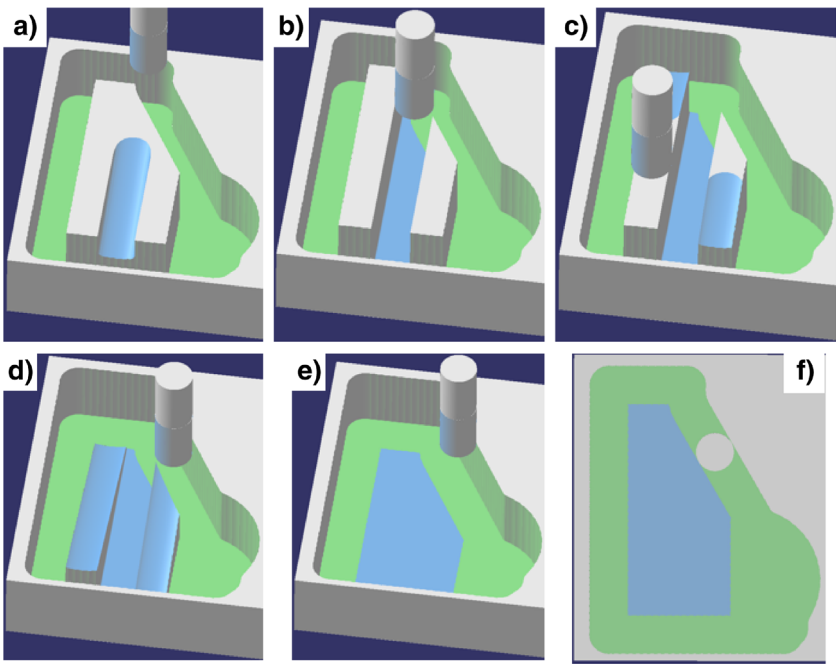

Fig. 14 Simulation of the material removal (orders of operations: from **a** to **f**)

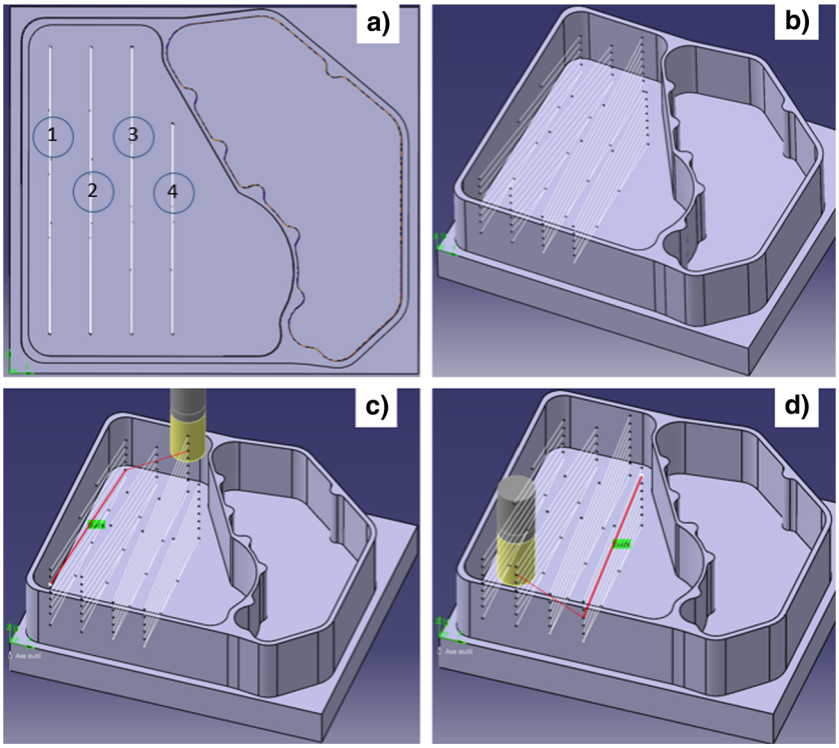

Fig. 15 Plunge milling and BotTCF ramping: 4 planes

HBR strategy with four BotTCF Ramping planes (Fig. 15). Two successive rectangular cycles of ramping trajectories are used: a rectangular cycle involving planes 1 and 3, followed by a rectangular cycle involving planes 2 and 4. This permits to reduce significantly the time associated with the cutter movements outside the material (carried out in rapid motion). An overall simulation representing the successive steps of milling with the HBR process along the four planes is displayed on Fig. 16.

Remarks:

– The BotTCF Ramping planes in the middle of two other planes cannot be larger than these planes, otherwise rectangular cycles of ramping trajectories cannot be

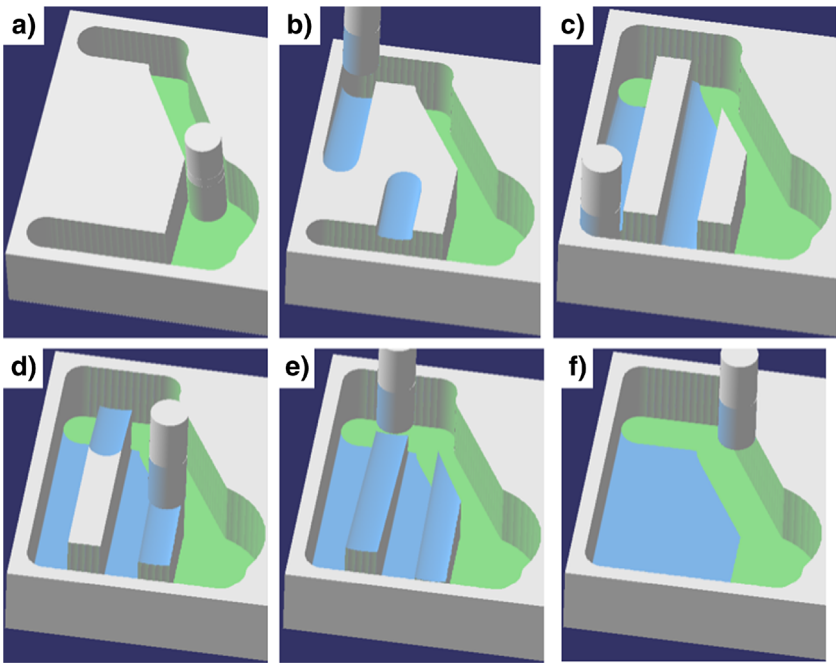

Fig. 16 Simulation of the material removal: 4 planes (orders of operations: from **a** to **f**)

used. In the first phase of the HBR methodology, plunge milling begins to remove material along the pocket walls. Then, plunge milling is again applied to obtain a remaining stock which guaranties that the BotTCF Ramping planes have the good dimensions (and then avoid interferences)

– If the material associated with the BotTCF Ramping plane (see the two islands on Fig. 16c) is not stiff enough (example: small-width remaining material (L_a) compared with the height of the stock), vibrations can appear and damage the cutter. One solution is to apply BotTCF Ramping at successive depth levels, so as to ensure sufficient stiffness. Note that the cutter trajectories do not need to be recomputed, as they are simply translated vertically from one level to the next.

For the second pocket in our example (Fig. 12), once plunge milling is completed along the pocket walls (Fig. 17a, b), the remaining stock features a small width and a rather irregular shape (Fig. 17c, d). In this case, BotTCF Ramping is inefficient. The remaining material is then removed with plunge milling. Indeed, HBR is efficient if the width of the stock is large enough compared with the diameter of the pocket milling cutter (case of pocket 1).

In the next section, we present the cutting-force models that permit to evaluate the forces acting on the plunge milling cutter and on the pocket milling cutter. These models are used later to determine the cutting conditions.

4 Cutting-force models

In order to perform a comparison of plunge milling with the proposed HBR method, we need cutting-force models that permit to evaluate the forces acting on the plunge milling cutter and on the pocket milling cutter. We first describe the model for plunge milling and then the one associated with BotTCF for the MRI301F material to be machined.

4.0.1 Plunge milling

In this subsection, we describe the model proposed in [8] used in our application. The authors propose a cutting-force model for plunge milling of magnesium-rare earth alloys. They consider the case of a dry plunge milling process applied to two wrought Mg- Zr-Zn-RE alloys (including MRI301F), and one cast Mg-Zr-Zn-RE alloy. Both are representative of the magnesium-rare earth alloys used in the aerospace industry.

In plunge milling, with the AQX milling cutter and this Mg-Zr-Zn-RE alloy, the radial force is negligeable [8]. Then, the only cutting forces to be considered are the tangential and axial forces. In this case, plunge milling behaves like orthogonal cutting, at each angular position of the insert. The effects of temperature are considerably less than for hard materials such as titanium alloys [17]. The cutting force model is then based on Merchant's orthogonal cutting model, adapted to the case of plunge milling to represent the axial and tangential cutting forces [8]. This model takes the non-null edge radius of the cutting inserts into account.

At each angular position of the insert, the tangential and axial cutting force models satisfy the following equations:

$$\begin{cases} Ft = \dfrac{2 \cdot \tau \cdot fz \cdot w(\theta) \cdot \cos(\varphi - \gamma_{mean})}{1 - sin(\varphi - \gamma_{mean})} \\ Fa = \dfrac{2\tau \cdot fz \cdot w(\theta) \cdot \sin(\varphi - \gamma_{mean})}{1 - sin(\varphi - \gamma_{mean})} \end{cases} \tag{3}$$

In these equations, $w(\theta)$ is the chip width, which changes with each angle of engagement, θ, of the insert into the material. The chip width is defined by Eq. 4.

$$w(\theta) = R + ae \cdot \sin\theta - \sqrt{R^2 - ae^2 \cdot \cos^2\theta} \tag{4}$$

The coefficient φ represents the angle of friction, and τ is the shearing stress. These coefficients are not constant, contrary to Merchant's hypothesis and evolve as a function of the cutting conditions. In Eq. 3, γ_{mean} is a mean rake angle

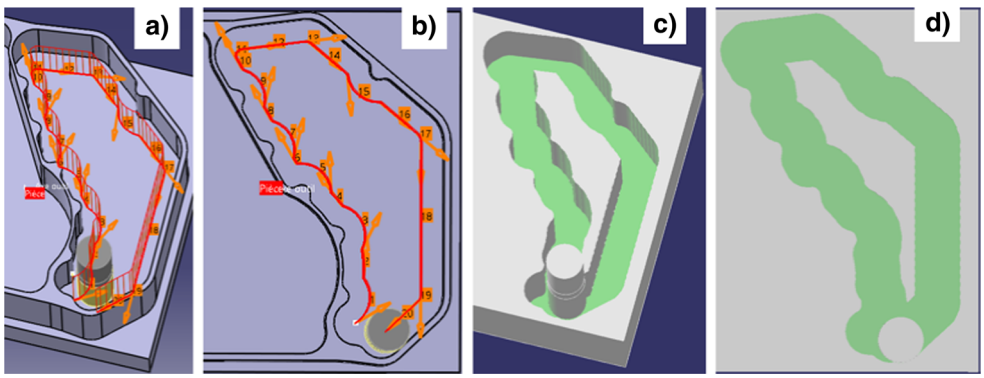

Fig. 17 Case where BotTCT Ramping cannot be applied efficiently

taking into account the non-null edge radius of the cutting inserts.

Hence, the system of Eq. 3 has two unknowns (τ and φ), at each angular position θ of the insert. The identification of these coefficients is determined using a non-linear least squares method based on three experimental tests. In the case of MRI301F, these coefficients are expressed by:

$$\begin{cases} \tau = 135,81 f z^{-0,1698} \\ \varphi = 0,3059 f z^{-0,1445} \left(\dfrac{Vc}{V_{c_0}}\right)^{-0,3306} \end{cases} \tag{5}$$

where V_{c_0} represents the minimum speed used in our tests.

4.0.2 BotTCF: balancing of the transversal cutting force

In this subsection, we describe the model proposed in [14] and used in our application. The authors propose applying BotTCF to pocket milling cutters. Their goal is to determine the optimal inclination of the cutter axis, so as to minimize the transversal cutting force. In order to find this optimal inclination, a new cutting force model is developed, tailored to the pocket milling cutters. Then, the BotTCF methodology is applied to this type of cutter. Finally, an experimental validation is carried out for the MRI301F alloy.

When milling with BotTCF, using the AXD7000 pocket milling cutter and the material MRI301F, the preponderant force is the tangential force [14].

The total tangential cutting force is the sum of two components:

$$Ft(\theta) = Ft_{int}(\theta) + Ft_{0-\pi}(\theta) \tag{6}$$

Using the BotTCF method leads to distinguish two cutting zones on the inserts: the interior and the exterior zones.

The force $Ft_{0-\pi}$ is the total force acting on the angular domain $[-\theta_e;\pi+\theta_e]$ (where θ_e is the cutter's angle of entry into the material), due to both the interior and exterior of the insert:

$$Ft_{0-\pi}(\theta) = Kt_{0-\pi}(\theta) \cdot S_{0-\pi}(\theta) \tag{7}$$

with

$$Kt_{0-\pi}(\theta) = K_{0_{0-\pi}} \cdot (e_{moy,0-\pi}(\theta))^{\beta_{0-\pi}} \tag{8}$$

The force $Ft_{int}(\theta)$ is the tangential cutting force acting on the insert interior, calculated on the angular domain $[\pi + \theta_e;2\pi - \theta_e]$:

$$Ft_{int}(\theta) = Kt_{int}(\theta) \cdot S_{int}(\theta) \tag{9}$$

with

$$Kt_{int}(\theta) = K_{0_{int}} \cdot (e_{moy,int}(\theta))^{\beta_{int}} \tag{10}$$

The tangential forces are expressed as the product of a specific cutting pressure and the instantaneous chip cross-section seen by the insert. In the above equations, $K_{0_{int}}$, β_{int}, $K_{0_{0-\pi}}$ and $\beta_{0-\pi}$ are coefficients, and $e_{moy,0-\pi}(\theta)$, $e_{moy,int}(\theta)$ are mean chip thicknesses at the angular position θ of the insert.

The radial and axial cutting forces, $Fr(\theta)$ and $Fa(\theta)$, are proportional to $Ft(\theta)$. However, the proportionality coefficients are not necessarily the same when the interior insert is machining alone or when it is machining with the exterior insert. We therefore have on the angular domain $[-\theta_e;\pi + \theta_e]$:

$$\begin{cases} Fr = Kr_{0-\pi} \cdot Ft \\ Fa = Ka_{0-\pi} \cdot Ft \end{cases} \tag{11}$$

and on the angular domain $[\pi + \theta_e;2\pi - \theta_e]$:

$$\begin{cases} Fr = Kr_{int} \cdot Ft \\ Fa = Ka_{int} \cdot Ft \end{cases} \tag{12}$$

where:

$$\begin{cases} Kr = \dfrac{Fr_{max}}{Ft_{max}} \\ Ka = \dfrac{Fa_{min}}{Ft_{max}} \end{cases} \tag{13}$$

The values of the coefficients $K_{0_{int}}$, β_{int}, $K_{0_{0-\pi}}$ and $\beta_{0-\pi}$ are set using least-squares regression with logarithmic residues. The coefficient Kr_{int} and $Kr_{0-\pi}$ are defined as proportionality coefficients between the maximum value of the experimental tangential cutting force Ft_{exp} and the maximum value of the experimental radial cutting force Fr_{exp}:

$$Kr_{int} = \frac{max(Fr_{exp})}{max(Ft_{exp})} \tag{14}$$

$$Kr_{0-\pi} = \frac{max(Fr_{exp})}{max(Ft_{exp})} \tag{15}$$

The coefficient Ka_{int} and $Ka_{0-\pi}$ are also defined as proportionality coefficients. For the MRI301F, the coefficients are:

$$\begin{cases} \beta_{int} = -0.1663 \cdot \alpha + 0.1455 \cdot fz \\ \qquad + 0.0672 \cdot a_p + 0.8531 \\ K_{0_{int}} = 1411.1 \cdot \alpha^{-1.2657} \cdot fz^{-0.169} \cdot a_p^{0.536} \\ \beta_{0-\pi} = 0.0131 \cdot \alpha - 0.339 \cdot fz \\ \qquad - 0.0129 \cdot a_p + 0.1378 \\ K_{0_{0-\pi}} = 282.197 \cdot \alpha^{-0.319} \cdot fz^{-0.475} \cdot a_p^{0.136} \\ Kr_{int} = 0.1002 \cdot ln(fz) + 0.0314 \cdot \alpha \\ \qquad - 0.0105 \cdot a_p + 0.138 \\ Kr_{0-\pi} = -0.0443 \cdot ln(fz) + 0.0326 \cdot \alpha \\ \qquad - 0.0183 \cdot a_p + 0.0493 \\ Ka_{int} = -0.2213 \cdot fz - 0.0036 \cdot \alpha \\ \qquad - 0.0058 \cdot a_p + 0.0629 \\ Ka_{0-\pi} = -0.2077 \cdot fz - 0.0344 \cdot \alpha \\ \qquad + 0.0181 \cdot a_p + 0.1021 \end{cases} \tag{16}$$

Note that α is expressed in degrees in these expressions. To use the above force models, it remains to provide the α value. This value is evaluated as follows.

The cutting forces Fx, Fy, Fz are expressed in the fixed reference framework. The values of Ft, Fr, Fa are defined by solving the following system of equations:

$$\begin{cases} Fx = Fr \cdot \cos\theta - Ft \cdot \sin\theta \\ Fy = Fr \cdot \cos\alpha \cdot \sin\theta + Ft \cdot \cos\alpha \cdot \cos\theta \\ Fz = Fr \cdot \sin\alpha \cdot \sin\theta + Ft \cdot \cos\theta \cdot \sin\alpha \\ \qquad + Fa \cdot \cos\alpha \end{cases} \tag{17}$$

Selecting the feed movement in the Y direction, the transversal cutting force is Fx. From Eq. 17, it can be seen that the transversal cutting force $Fx(\theta)$ does not depend on the axial force $Fa(\theta)$. The total transversal cutting force acting on the cutter is the sum of the transversal cutting forces of the inserts [12]. More precisely, the transversal cutting force for a cutter with two teeth, noted Fx_{2teeth}, is the sum of the cutting force computed at a position θ and the force computed at a position $\theta + \pi$:

$$Fx_{2teeth}(\theta) = Fx(\theta) + Fx(\theta + \pi) \tag{18}$$

To simplify the notations, in the rest of the paper, $Fx_{2teeth}(\theta)$ is simply noted $Fx(\theta)$. Thus, to define the balance angle $\alpha = \alpha_{eq}$, the minimum and maximum values, Fx_{min} and Fx_{max}, of the transversal cutting force $Fx(\theta)$ are computed in such a way that the following equilibrium equation is satisfied:

$$Fx_{max} = -Fx_{min} \tag{19}$$

In the next section, we discuss the performances of the HBR method on a real-life closed deep pocket.

5 Experimental validation and results

In this section, we compare the HBR method with plunge milling on a closed deep pocket of a simplified aeronautical housing made of magnesium-rare earth alloy.

This section is organized as follows. The first subsection describes the experimental protocol (cutters, CNC machine tool, material, range of cutting conditions, and the workpiece dimensions). In the second subsection, we define the admissible maximum force on cutters. For making a fair machining-time comparison of plunge milling with the proposed HBR method, the admissible maximum force has to be the same on both the plunge milling cutter and the pocket milling cutter. This admissible maximal force is determined from accoustic measurement tests and recorded tests with a high-speed camera. In the third subsection, we use the admissible maximum force on cutters and the cutting force models to define the most efficient cutting conditions for plunge milling and BotTCF Ramping. The last subsection defines the trajectories of plunge milling and BotTCF Ramping, and reports the results in term of machining-time comparison of plunge milling with the HBR strategy.

Table 1 DMU 50 kinematic characteristics

Parameter	A^M	J^M	V_R^M	V_f^M
Units	m/s^2	m/s^3	m/min	m/min
Value	4.9	40	50	24

5.1 Experimental protocol

The machined material is a magnesium-rare earth alloy MRI301F (Mg-Nd-Y-Zr-Zn). It is a very light material (density: approximatively 1800 kg/m^3), featuring high strength, good corrosion resistance, and can be used under high-temperature conditions. Cutting forces are measured with a Kistler six-component force measurement plate 9257B. The tests are performed on a DMU 50 eVolution 5-axis machine (with a Siemens 840D CNC controller), without lubrication. The mainly kinematic characteristics of the DMU 50 eVolution are defined (for each axis) by its maximum axis acceleration reachable A^M, its maximum axis jerk J^M, its maximum rapid speed V_R^M, and its maximum axis speed reachable V_f^M. Their values are given in Table 1. For the tests carried out in this study, the value of the jerk is set to $J^M = 40$ m/s^3.

The plunge-milling tests are performed with a 33 mm diameter Mitsubishi AQX milling cutter with two teeth. This cutter is a center-cut end mill. The HTi10 grade inserts have a polished rake face with a very sharp edge and are designed for the machining of non-ferrous alloys. These inserts have a rake angle of 22.5°. Their edge radius is equal to 2.5 μm.

The BotTCF Ramping tests are performed with a pocket milling cutter with two teeth. The cutting tool used is a 32 mm diameter Mitsubishi AXD7000 milling cutter with TF15 grade inserts. They have also a polished rake face and a very sharp edge (about 2.5 μm) as the inserts of the AQX milling cutter. The insert nose radius is equal to r=1.6 mm.

Due to confidential issues, the values for the cutting speed Vc (m/min) and the feed per tooth fz (mm/rev/tooth) are not given here. They are stated in MRI301F as a percentage of the cutting conditions Vc^* and f^* given by Mitsubishi for these cutters in non-ferrous alloys (Table 2). In this paper, the cutting conditions of the MRI301F are then normalized in the range [–1, +1]. In the sequel, when the (unitless) value of Vc is 0.5, we shall denote this value

Table 2 Variation ranges of cutting conditions with HTI10 and TF15 inserts

	Forged MRI301F	
Vc	80% to 200% of Vc^*	-1 to $+1$
fz	154% to 1000% of f^*	-1 to $+1$

$Vc + 0.5$ to emphasize the fact that it is a normalized value of the cutting speed. In an analogous manner, the feed per tooth values are also normalized in the intervall $[-1, +1]$ with the same notational unitless convention. The bounds of the design of experiments are shown in Table 2.

Some measurements of sound intensity are carried out during the milling tests. The sounds are recorded using a Handy recorder-zoom H4 equipped with two microphones. A high-speed PHOTRON camera (type: APX-RS) is also used (Fig. 18). This camera provides full mega pixel resolution images (1024 × 1024 pixels) at up to 3000 frames per second (fps), 512 × 512-pixels resolution at 10,000 fps, and at reduced frame rates to an unrivaled frame rate of 250,000 fps.

The experimental set-up is shown in Fig. 18.

The test workpiece, a simplified aeronautical housing made of MRI301F (see Figs. 12 and 25), has the following dimensions: 300 mm × 270 mm, height of pockets: 60 mm.

5.2 Admissible maximum cutting force (dynamic cutter behavior)

In this subsection, we define an identical maximum cutter loading level for the two cutters, the one used in plunge milling and the one used in BotTCF, respectively. For this purpose, we use the cutting force models defined in the above subsection. Due to both cutter limitations (bending, stiffness, vibrations, wear) and maximum loading on machine-tool axis, the cutting forces have to be below some critical values. From the cutting force models presented in the previous subsections, the preponderant force, for the MRI301F, is the tangential force for both plunge milling and milling with BotTCF. The axial and radial forces acting on the cutters are much less important than the tangential force. We take as maximum cutter loading level, the maximum value of the resulting force $F_R = \sqrt{Ft^2 + Fr^2 + Fa^2}$. This maximum cutter loading level is noted $F_{R_{max}}$. In order to determine the maximum allowable value for the resulting force, we use accoustic measurement tests and recorded tests with a high-speed camera. For the two milling processes, these measurements allow one to evaluate the maximum value of the resulting cutting force corresponding to a dynamic behavior satisfying the cutter limitations mentioned above.

Fig. 18 Experimental set-up

Some measurements of sound intensity are carried out during machining, in order to compare the two milling processes, plunge milling and BotTCF Ramping. Relative sound intensity is an extremely effective indicator to quantify the chatter produced during machining. Thus, the comparison criterium retained is the relative acoustic power [12]. The acquisition frequency used is 44.1 kHz for sound recording. Recorded sounds in stationary mode are processed using the Scilab 4.1 software to conduct signal analysis. For these tests, relative acoustic power in dBs is calculated using the Weber-Fechner's law for comparative purposes [9, 12]. The tool-holder is a BT 40 tool-holder with a hydraulic chuck. For the two cutters, the cutter's length outside the tool-holder is about 65mm. This enables us to use stiffness values that are close to each other for the two cutters.

Table 3 shows, for two representative test cases, that the sound intensity associated to BotTCF Ramping is significantly lower than that associated to plunge milling. The relative reductions are about –4.46 dB for the first test, and about –9.1 dB for the second test. These examples show the better dynamic cutter behavior of pocket milling cutters when BotTCF Ramping is used. Therefore, using the same cutting conditions for the two milling processes, plunge milling corresponds to the most restrictive case. As a consequence, we set the maximum resulting cutting force to $F_{R_{max}}$=1250 N, that corresponds to an acceptable sound level during plunge milling. This value corresponds to a cutter behavior that does not exhibit significant vibrations, which could be harmful for the cutter inserts. This is verified using a high-speed camera (Fig. 18).

5.3 Cutting conditions

Given this common maximum resulting cutting force allowed ($F_{R_{max}}$=1250 N), in the next two subsections, we

Table 3 Calculated relative acoustic powers

ae (mm)	a_p (mm)	fz (normed)	Vc (normed)	Plunge milling (dB)	BotTCF Ramping (dB)
6	6	$fz + 1$	$Vc + 0.5$	−13.38	−17.84
9	9	$fz + 0.55$	$Vc + 0.5$	−10.4	−19.5

Table 4 Cutting conditions

	ae (mm)	a_p (mm)	fz (normed)	Vc (normed)
Plunge milling (walls)	6		$fz+0.67$	$Vc+0.5$
Plunge milling (interior)	9.2		$fz-0.27$	$Vc+0.5$
BotTCF Ramping		11	$fz+0.55$	$Vc+0.5$

compute the maximum cutting conditions for both processes (plunge milling and BotTCF Ramping).

5.3.1 Plunge milling

The pocket height of the test workpiece (a simplified aeronautical housing) considered in this study is slightly less twice the cutter diameter (60 and 33 mm, respectively), which corresponds to a usual cutter stiffness. Moreover, the CNC machine tool features standard dynamic characteristics (moderate acceleration and maximum axis speed reachable) (Table 1). This corresponds to a situation where the following simple heuristic can be applied for computing optimal cutting conditions (referred to as *SIS* in [2]). SIS proceeds as follows by setting successively each cutting condition: first, the radial offset value ae is set to its largest possible value (not exceeding the insert width), thereby minimizing the number of plunges. Here, this value is: ae=9.2 mm. Generally, the remaining cutting conditions (Vc, fz) are set so as to reach the maximum resulting cutting force threshold value, $F_{R_{max}}$=1250 N. In our case, the tangential force is particularly influenced by the feed per tooth, fz, and the radial offset, ae, weakly depends on the cutting speed. We set the value of the cutting speed in its admissible range: here we choose arbitrarily $Vc+0.5$. Then, the feed per tooth value is computed straightforwardly from Eq. 3. The obtained value is $fz-0.27$. In Eq. 3, the minimum speed is V_{c_0}=$Vc-1$. Figure 20 shows the tangential force and the axial force during plunge milling with these cutting conditions.

Remark that in both plunge milling and HBR processes, we are about to compare one needs to set a smaller radial offset value ae to avoid too rough remaining scallop material along the pocket walls. For both processes, we set this reduced ae value to 6 mm. Again, the remaining cutting conditions (Vc, fz) are set to reach the maximum resulting cutting force threshold value, $F_{R_{max}}$=1250 N: $fz+0.67$ and $Vc+0.5$. Table 4 summarizes the cutting conditions.

5.3.2 BotTCF ramping

In order to define the cutting conditions reaching the maximum resulting cutting force, one must distinguish two different milling zones: zone 1 (composed of two sub-zones: zone-1a and zone-1b) and zone 2. More precisely, zone 1 corresponds to the starting and ending parts of each trajectory, illustrated in red and in green colors respectively in Fig. 19. Zone 1 cannot be milled in a well-balanced manner since only one tooth at a time is milling (contrary to zone 2). In such an assymetrical situation, the cutting forces generated by one tooth can be important and one must ensure that the resulting cutting force does not go beyond $F_{R_{max}}$=1250 N. In zone 2, the two teeth are milling. In the first part (in violet color in Fig. 19), the depth of cut increases slowly until it reaches the constant value a_p used in the second part of the trajectory (in white color in Fig. 19). Therefore, the cutting conditions for the white trajectories are necessarily admissible for the violet trajectories in terms of maximum resulting forces. During the second part (with constant depth of cut a_p), the transversal cutting force can be balanced, using an optimal inclination angle α_{eq}, as in Eq. 19.

Let us compute cutting conditions (a_p, fz, Vc) that are valid for both zones. The a_p value must be chosen larger than the ae value (of plunge milling), otherwise one can show that in order to reach the maximum resulting cutting force threshold value, the fz value would be out of its validity range (Table 2). We choose to set a_p=11 mm. Although non optimal, this choice induces a reduction of the total number of trajectories compared to plunge milling.

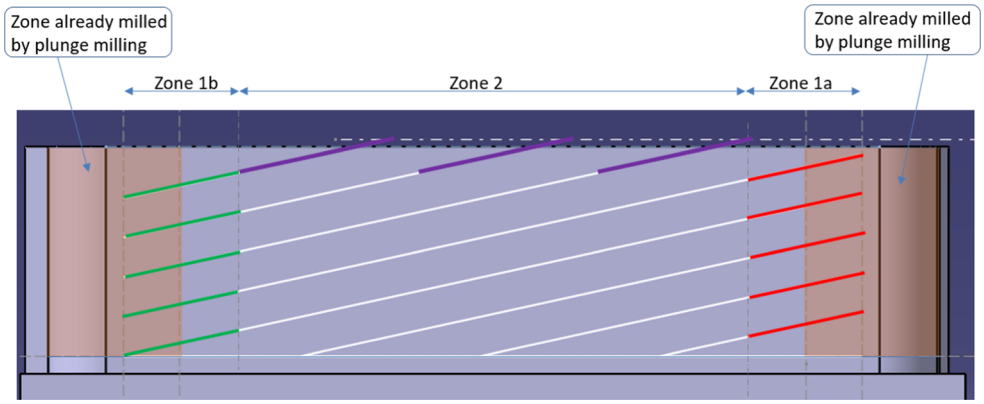

Fig. 19 The zones of BotTCF Ramping and the different sections of the cutter trajectories: *violet color* for two teeth in the material with a_p variable, *white color* for the part where the transversal cutting force can be balanced with two teeth in the material and a_p constant, *red color* for the starting part with one tooth removing the material, and *green color* for the ending part with one tooth removing the material

Considering the same cutting speed as for plunge milling, $Vc + 0.5$, we deduce the feed per tooth value: $fz + 0.55$. These cutting conditions are summarized in the last line of Table 4.

From these cutting conditions, the optimal inclination angle α_{eq} that best balances the transversal cutting force is equal to: α_{eq}=12.62°.

The corresponding maximum tangential, radial, and axial cutting forces are as follows:

- For one tooth cutting the material (zone 1): Ft=1136 N, Fr=450 N, Fa=253 N implying a resulting force equal to 1248 N.
- For two teeth cutting the material (zone 2): Ft=572 N, Fr=330 N, Fa=468 N implying a resulting force $F_{R_{max}}$ equal to 827 N. The minimum and maximum values of the transversal cutting force are equal to $Fx_{max} = -Fx_{min}$=364 N.

Remark that from the same constraint on the maximum cutting force, the cutting conditions obtained for BotTCF Ramping are substancialy higher (hence better) than the ones obtained for plunge milling (Fig. 20). This can be explained as follows. Due to the inclination angle involved in BotTCF Ramping, the teeth only remove the material progressively, contrary to milling without inclination in which case the full depth of cut a_p must be tackled at once. This feature is independant of whether the forces are well balanced or not, nor whether one tooth or two teeth are milling.

Another interesting remark is that the tangential force in zone 2 is reduced roughly by a factor two, and the resulting force by a factor 1.5. This is the main benefit obtained from using the BotTCF criterion.

Figure 21 shows the cutting forces (Ft, Fr, Fa) for one tooth, with α_{eq}=12.62°. Figure 22 shows the cutting forces Fx and Fy for two teeth, with the optimal inclination angle α_{eq}=12.62°.

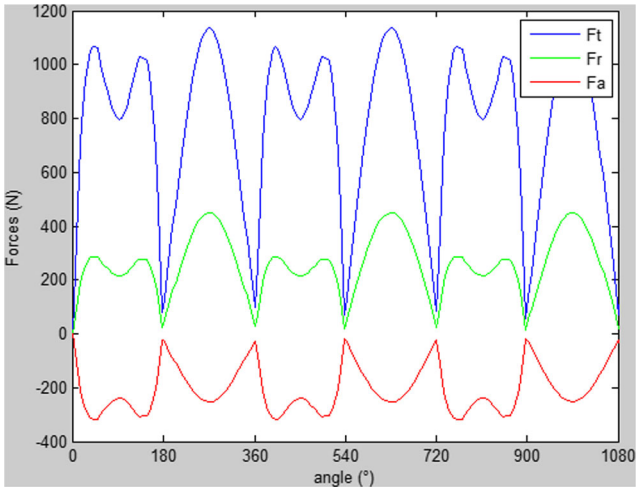

Fig. 21 Cutting forces (Ft, Fr, Fa) during BotTCF Ramping, for one tooth and α_{eq}=12.62°

5.4 Plunge milling and HBR trajectories

The test workpiece, a simplified aeronautical housing made of MRI301F (Fig. 12), has the following dimensions: 300 mm × 270 mm, height of pockets: 60 mm. The tool trajectories of the HBR method are defined in the study of the closed deep pockets (Section 3.2). It remains to define the trajectories of the plunge milling solution.

In order to define the plunge milling trajectories, we use the CATIA V5-R22 CAM software. CATIA proposes different strategies for roughing the workpiece (Fig. 23). The

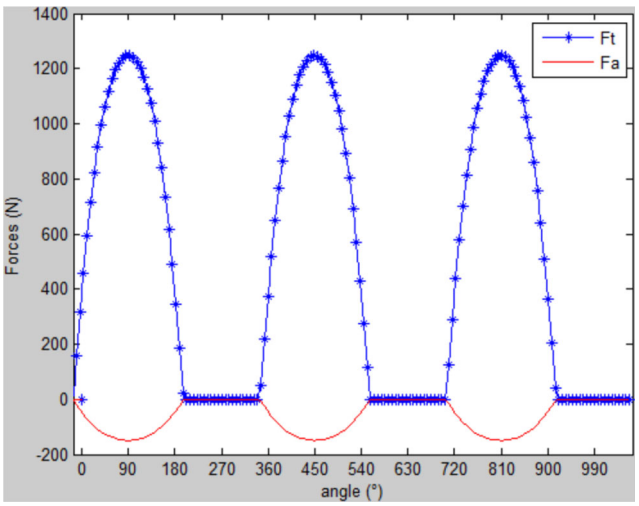

Fig. 20 Cutting forces (Ft, Fa) during plunge milling (ae=9.2 mm, $fz - 0.27$, $Vc + 0.5$)

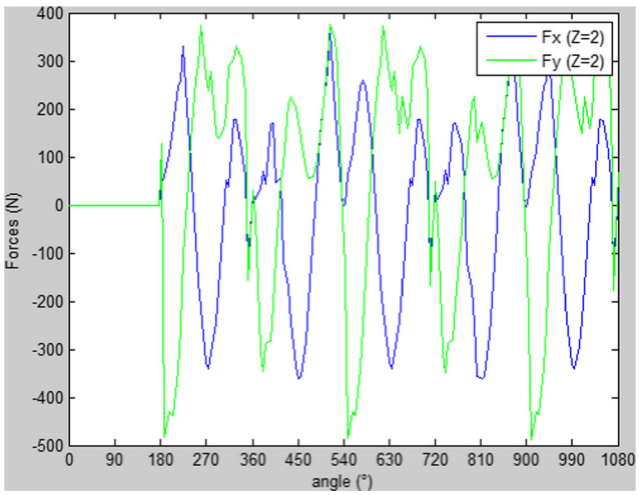

Fig. 22 Cutting forces (Fx, Fy) during BotTCF Ramping, for two teeth and α_{eq}=12.62°

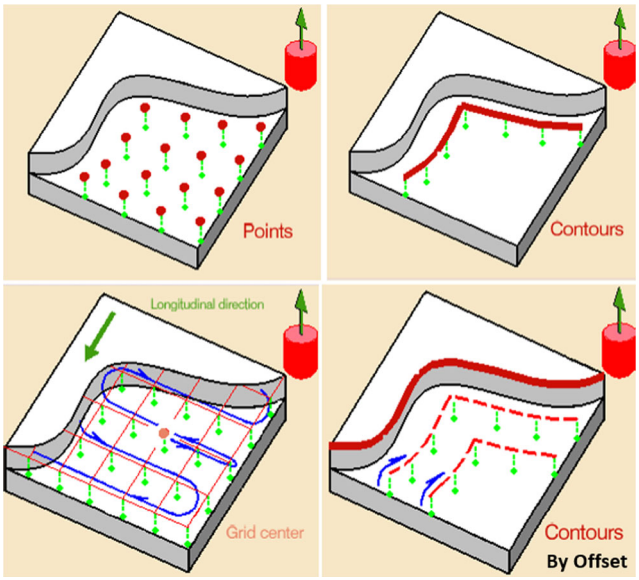

Fig. 23 CATIA V5 plunge milling strategies

plunge tool path positions are placed on a grid which is either:

- Rectangular, defined by two step values, a direction and a center point.
- Defined from selected points or from contours, defining the position and the order of machining.
- Defined by offsets from a selected contour.

Outside geometrically simple shapes for workpieces, the CAM software does not necessarily offer optimized trajectories. An alternative to improve the proposed automatic solutions is to create the trajectories that the cutter will follow. The most efficient CATIA V5 automatic solution in our case is the offset solution from the inside contour of each pocket. We have improved the automatic solution proposed by the software, sketching our own trajectories. The paths are sketched with the CAD module. The improved trajectories for the two pockets are shown in Fig. 24. They make it possible to mill each pocket by leaving no unmachined material or without returning on already machined areas.

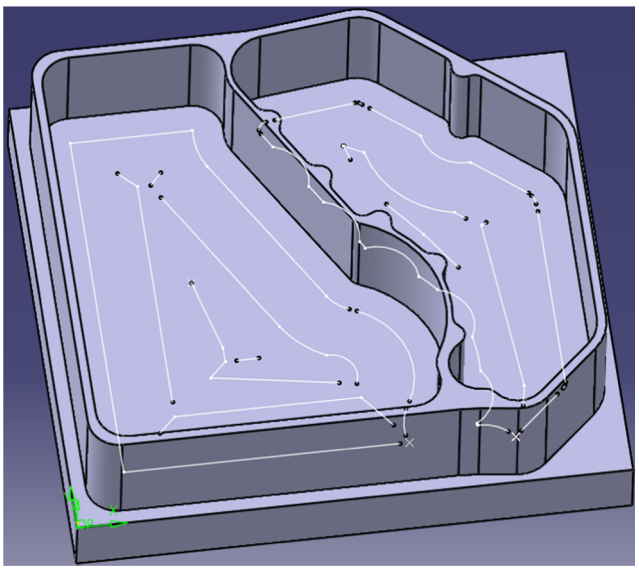

Fig. 24 Improved plunge milling trajectories

Table 5 Method 1 (plunge milling): machining times

	T (s)
Plunge milling (walls)	92.6
Plunge milling (interior roughing)	80.2
Total time	172.8

Manually improving trajectories (by drawing our own sketches) allows one to gain about 21.8% on the machining time compared to the automatic solution of Catia V5 on pocket 1, and 17.5% on pocket 2. The time comparisons are deduced from real machining times on the CNC machine tool. Indeed, simulated machining times provided by CAM software do not take into account the control laws of the CNC machine, and therefore underestimate the actual machining times [2]. This improved plunge milling solution will be the reference solution with which the HBR solution will be compared in the sequel of the paper. Let us now study the machining of the test workpiece by plunge milling and HBR method, and quantify the machining times.

5.5 Comparisons and results

Pocket 2 is milled only in plunge milling, due to the geometry and specific dimensions of the pocket. The gains of the new HBR method must then be quantified on pocket 1. Pocket 1, for its part, is milled by three different methods:

- Method 1: plunge milling
- Method 2: HBR with three planes (Figs. 13 and 14)
- Method 2: HBR with four planes (Figs. 15 and 16)

The tool change time is not counted because in the plunge milling solution, at the end of the roughing operation, the tool will be changed and replaced by the pocket milling cutter which will be used for the finishing operations (walls

Table 6 Method 2 (plunge milling and BotTCF Ramping with three planes): machining times

	T (s)
Plunge milling (walls)	92.6
Plunge milling (remachining)	16.5
BotTCF Ramping (3 planes)	42
Total time	151.1

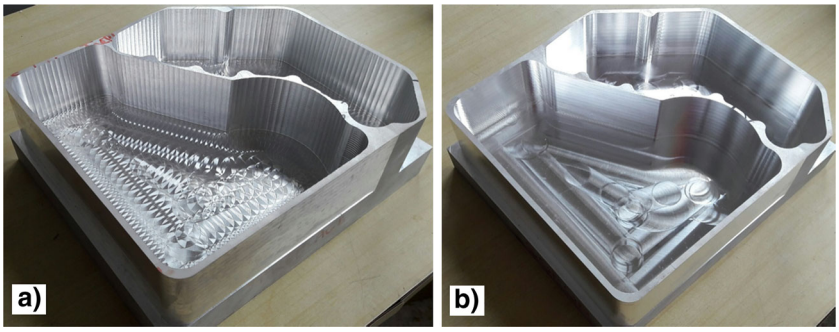

Fig. 25 Milled part: **a** after roughing **b** after finishing

and bottom of the pocket); in method 2, the cutter is already in the spindle at the end of the roughing. The time to rough the material along the walls is the same for the two methods and is equal to 92.6 s. After this first material removal, the remaining material is then milled. To do this, the roughing time for method 1 is 80.2 s (Table 5) and the roughing time for method 2 is 16.5+42=58.5 s (Table 6). The gain in time to remove the remaining material using method 2 is about 27%.

Remarks:

- In the case where one would consider a different cutter than the plunge milling cutter in order to perform the finishing operation, it would be necessary to take into account the tool change time (about 7 s). In this case, the gain in time using method 2 is more than 18%. In all cases, the gain using method 2 remains important.
- For method 2, during BotTCF Ramping, we could have decomposed each straight-line elementary trajectory of the cutter into three parts: starting (zone 1a), middle zone (zone 2), and ending (zone 1b). This could have permit to improve the feed per tooth in zone 2 (Fig. 19) where the transversal cutting force can be balanced, which would have led to an even greater increase in the time savings compared with method 1.

Figure 25a shows one of the two parts machined in roughing. Figure 25b shows a workpiece completely machined after finishing operations.

Method 3 is only simulated (the workpiece was not machined). Nevertheless, the machining times were recorded on the machine (Table 7) in order to be able to verify and to quantify the time saving brought by this method, where the cutter movements outside the material are even more reduced by using two successive rectangular cycles of ramping trajectories.

Table 7 Method 3 (plunge milling and BotTCF Ramping with four planes): machining times

	T (s)
Plunge milling (walls)	65.3
Plunge milling (remachining)	16.5
BotTCF Ramping (4 planes)	50.8
Total time	132.6

In the case of method 3, all the walls of pocket 1 are not plunge milled (Fig. 16a). One of these walls is milled with BotTCF Ramping. The roughing time for method 3 is equal to 50.8+16.5+(92.6−65.3)=40 s.

The gain in time using method 3 compared with method 1 is about 50%. The gain in time using method 3 compared with method 2 is more than 31%.

Remark that if the width of the pocket is sufficient, enabling the installation of several planes, the new methodology allows one even more substantial gains compared with plunge milling.

Now, considering the gains on the total machining time, taking into account all the operations, it results that the gain in time using method 2 compared with method 1 is more than 12%, and the gain in time using method 3 compared with method 1 is about 23%.

6 Conclusions

In this paper, we have extended the BotTCF concept to roughing deep pockets: open pockets and semi-open pockets opened from side to side. A new hybrid methodology for roughing semi-open and closed pockets has been developed. This new hybrid methodology is based on the combination of plunge milling and ramping trajectories using the BotTCF criterion. The proposed methodology has been developed for three-axis machining and can be extended to five-axis machining. For very deep pockets, one solution is to apply plunge milling and BotTCF Ramping at successive depth levels. The cutter trajectories are defined on a first height. When this first material removal has been done, the previous cutter trajectories are translated downwards, along the Z-axis of the machine, without new calculation.

BotTCF Ramping provides several advantages over plunge milling:

- Most of the trajectories are longer than in plunge milling. Such long trajectories make it possible to achieve a high programmed feedrate V_f for a longer time, thus reducing the machining time. Indeed, in the case of machining magnesium alloy parts, the programmed feedrates are very high. The axis motions of the CNC machine tool are driven by constant jerk steps, and a certain amount of time is required to reach the programmed feedrate. This programmed feedrate can thus be maintained for a longer time with long trajectories exhibiting fewer discontinuities.
- The lengths of the cutter movements outside the material (carried out in rapid motion) are smaller when using rectangular cycles of ramping trajectories than in plunge milling.
- From the same constraint on the maximum cutting force, we have seen that the cutting conditions obtained for BotTCF Ramping are substantially better than those obtained for plunge milling. This is due to the inclination angle involved in BotTCF Ramping. In the zone where the transversal cutting force can be well balanced, the cutting conditions can be improved: the feed per tooth can be increased.

Without decomposing each trajectories in three parts and applying different cutting conditions on them, the HBR method has shown its efficiency for roughing deep pockets. Gains from 12 to 23% on the total machining time have been obtained for one pocket, in comparison with plunge milling which is recognized as an efficient process to rough deep pockets. In the HBR methodology, once plunge milling is achieved, the remaining stock that is milled with BotTCF Ramping can be considered like an open deep pocket. Gains as high as 27% for method 2 or 50% for method 3 have been obtained in comparison with plunge milling (method 1). We then see that for open pockets, the gains in machining time can be significant. Future research will extend this work for materials other than magnesium alloys and will take into account trajectories with different feedrates to take maximum advantage of the BotTCF Ramping strategy.

Acknowledgments The authors would like to thank the CARAIBE project, which is supported by french national funds (FUI) and the Aerospace Valley cluster.

References

1. Rauch M, Hascoet J-Y (2012) Selecting a milling strategy with regard to the machine tool capabilities: application to plunge milling. Int J Adv Manuf Technol 59(1–4):47–54
2. Cafieri S, Monies F, Mongeau M, Bes C (2016) Plunge milling time optimization via mixed-integer nonlinear programming. Comput Ind Eng 98:434–445
3. Ko JH, Altintas Y (2006) Dynamics and stability of plunge milling operations. J Manuf Sci Eng 129(1):32–40
4. Ko JH, Altintas Y (2007) Time domain model of plunge milling operation. Int J Mach Tools Manuf 47(9):1351–1361
5. Altintas Y, Ko JH (2006) Chatter stability of plunge milling. CIRP Ann Manuf Technol 55(1):361–364
6. Danis I, Wojtowicz N, Monies F, Lamesle P, Lagarrigue P (2013) Cutting conditions and surface integrity during dry plunge-milling of a wrought magnesium alloy. Procedia Engineering 63:36–44
7. Danis I, Wojtowicz N, Monies F, Lagarrigue P (2014) Influence of dry plunge milling conditions on surface integrity of magnesium alloys. International Journal of Mechatronics and Manufacturing Systems 7(2–3):141–156
8. Danis I, Monies F, Lagarrigue P, Wojtowicz N (2016) Cutting forces and their modelling in plunge milling of magnesium-rare earth alloys. Int J Adv Manuf Technol 84(9):1801–1820
9. Gilles P, Cohen G, Monies F, Rubio W (2012) Torus cutter positioning in five-axis milling using balance of the transversal cutting force. Int J Adv Manuf Technol 66(5–8):965–973
10. Gilles P, Cohen G, Monies F, Rubio W (2014) Machining strategy in five-axis milling using balance of the transversal cutting force. Int J Adv Manuf Technol 72(9–12):1377–1387
11. Gilles P, Monies F, Rubio W (2007) Optimum orientation of a torus milling cutter: method to balance the transversal cutting force. Int J Mach Tools Manuf 47(15):2263–2272
12. Gilles P, Cohen G, Monies F, Rubio W (2008) Dynamic behaviour improvement for a torus milling cutter using balance of the transversal cutting force. Int J Adv Manuf Technol 40(7–8):669–675
13. Moussaoui K, Monies F, Mousseigne M, Gilles P, Rubio W (2015) Balancing the transverse cutting force during inclined milling and effect on tool wear: application to Ti6al4v. Int J Adv Manuf Technol 1–22
14. Monies F, Danis I, Lagarrigue P, Gilles P, Rubio W (2017) Balancing of the transversal cutting force for pocket milling cutters: application for roughing a magnesium-rare earth alloy. Int J Adv Manuf Technol 89(1):45–64
15. Sandvik (2012) Plunge milling - how to apply. http://www.sandvik.coromant.com/en-gb/knowledge/milling/application_overview/holes_and_cavities/plunge_milling/Pages/ default.aspx
16. Sun C, Bi Q, Wang Y, Huang N (2014) Improving cutter life and cutting efficiency of five-axis plunge milling by simulation and tool path regeneration. Int J Adv Manuf Technol 77(5–8):965–972
17. Sun T, Fu Y-c, He L, Chen X-m, Zhang W-g, Chen W, Su X-b (2016) Machinability of plunge milling for damage-tolerant titanium alloy TC21. Int J Adv Manuf Technol 85(5–8):1315–1323